Received 14 February 2019; revised 26 April 2019; accepted 1 May 2019. Date of publication 6 May 2019; date of current version 24 May 2019.
The review of this paper was arranged by Editor S. Vaziri.

Digital Object Identifier 10.1109/JEDS.2019.2915028

A Fully Printed Ultra-Thin Charge Amplifier for On-Skin Biosignal Measurements

MIKA-MATTI LAURILA [1], HIROYUKI MATSUI [2], REI SHIWAKU [2], MIKKO PELTOKANGAS [3], JARMO VERHO [3], KAREM LOZANO MONTERO [1], TOMOHITO SEKINE [2], ANTTI VEHKAOJA [3], NIKU OKSALA [3,4,5], SHIZUO TOKITO [2], AND MATTI MÄNTYSALO [1] (Member, IEEE)

1 Faculty of Information Technology and Communication Sciences, Tampere University, 33720 Tampere, Finland
2 Research Center for Organic Electronics, Yamagata University, Yonezawa 992-8510, Japan
3 Faculty of Medicine and Health Technology, Tampere University, 33720 Tampere, Finland
4 Vascular Surgery and Interventional Radiology Centre, Tampere University Hospital, 33521 Tampere, Finland
5 Finnish Cardiovascular Research Center Tampere, 33521 Tampere, Finland

CORRESPONDING AUTHOR: M.-M. LAURILA (e-mail: mika-matti.laurila@tuni.fi)

This work was supported in part by the Academy of Finland under Grant 310617, Grant 310618, and Grant 320019, in part by the Japan Society for the Promotion of Science LEADER Program, and in part by the Japan Science and Technology Agency OPERA Program. The work of A. Vehkaoja was supported by the Academy of Finland under Grant 292477. The work of M. Mäntysalo was supported by the Academy of Finland under Grant 288945 and Grant 319408.

ABSTRACT In this contribution, we propose a fully printed charge amplifier for on-skin biosignal measurements. The amplifier is fabricated on an ultra-thin parylene substrate and consists of organic transistors, integrated bias and feedback resistors, and a feedback capacitor. The fabrication process utilizes inkjet-printed Ag ink for source, drain, gate, and capacitor electrode metallization as well as for the interconnects between the amplifier elements. Dispensed polystyrene, 2,7-dihexyl-dithieno[2,3-d;2',3'-d']benzo[1,2-b;4,5-b']dithiophene (PS:DTBDT-C6), is used as the transistor channel material, dispensed poly(3-hexylthiophene) (P3HT) as the high-resistivity material for the printed resistors, and parylene as the capacitor dielectric. A pass band optimized for pulse-wave measurement (60 mHz to 36 Hz) is achieved with a maximum charge amplification of 1.6 V/nC. To demonstrate the potential of the proposed printed amplifier, a radial arterial pulsewave signal recorded with a printed piezoelectric poly(vinylidenefluoride-co-trifluoroethylene) (PVDF-TrFE) sensor was fed to it and the output was analyzed to quantify the similarity of the pulse-wave features calculated from the original signal and the amplifier output. The amplified signal contains all the essential features of a pulse wave, such as both systolic waves, the dicrotic notch, and diastolic wave, which enable the accurate derivation of the clinically relevant indices utilized in the evaluation of vascular health.

INDEX TERMS Printed electronics, ultra-thin amplifier, charge amplifier, biosignal amplifier, electronic skin, lab-on-skin, arterial pulse wave measurement.

I. INTRODUCTION

Recently there has been rapid progress in the field of on-skin biosignal measurements [1], and at the center point of this progress has been the development of ultra-thin sensors for electrocardiography (ECG) [2], [3], electroencephalography (EEG) [3], electromyography (EMG) [3], [4], and electro-oculography (EOG) [3], [5], as well as for temperature [6], chemical [7], and arterial pulse-wave measurements [8], [9]. A fully-fledged lab-on-skin setup [10] may also require antennas for data transfer, an energy supply for powering active components [11], [12], preamplifiers for amplifying the otherwise weak biosignals [13], and ultra-thin conductors for providing the connection between the components [3]. The ultra-thin form factor of the lab-on-skin setup is vital for achieving high skin conformability and enhanced user comfort. Furthermore, it provides more direct coupling between the sensor and the biosignal because the attachment to the skin takes place via van der Waals forces instead of adhesives, which may attenuate the signal. However, the minimal thickness of the devices also makes them very fragile and difficult to re-use, thus in practice, causing

them to be disposable. Additive direct printing technologies offer an ideal solution for this problem since they are low cost, have minimal material consumption, and are able to maintain the ultra-thin form factor.

However, this presupposes that all components can be fabricated using printing technologies, which is not necessarily the case. For example, preamplifiers using organic thin-film transistors on ultra-thin substrates have previously been developed [7], [13], [14] but they generally use external feedback resistors and capacitors, which are bulky and have to be separately connected to the circuit. Replacing these components with additively fabricated thin-film counterparts is therefore important for the implementation of a truly ultra-thin lab-on-skin setup. So far, printed resistors have been fabricated using pristine and doped poly(3,4-ethylenedixothiophene)-poly(styrenesulfonate) (PEDOT:PSS) [16] and PEDOT:PSS mixed with poly(methyl methacrylate) (PMMA) [17], but the process variation makes them questionable for integration with printed amplifier circuits. A few amplifier demonstrators with integrated PEDOT:PSS resistors exist [18], [19], but the reproducibility of their fabrication has not been studied in depth.

In order to increase the reproducibility of the resistor fabrication, we employed a novel type of resistor structure with inkjet-printed silver (Ag) electrodes, dispensed Teflon surface-energy patterns, and dispensed, high-resistivity pristine poly(3-hexylthiophene) (P3HT) [20] in order to miniaturize the physical size of the resistor as much as possible and accurately control its dimensions. Furthermore, we use inkjet-printed Ag electrodes and a parylene dielectric to fabricate parallel plate capacitors with high reproducibility. As a technology demonstrator, we integrated these resistors and capacitors into a fully printed, ultra-thin amplifier as bias and feedback components and showed that the circuit has acceptable gain-bandwidth characteristics for amplifying an arterial pulse-wave signal recorded with a piezoelectric poly(vinylidenefluoride-co-trifluoroethylene) (PVDF-TrFE) pressure sensor. The amplified pulse-wave signal was analyzed for essential features, and clinically relevant indices were calculated based on these. The maximum thickness of the printed circuit is approximately 3 μm, making it a truly ultra-thin setup.

II. MATERIALS AND METHODS

A. THE AMPLIFIER FABRICATION PROCESS

Carrier substrates were cut from sheet glass of 0.7 mm thickness. Fluoropolymer Teflon (AF1600X, Chemours Inc.) was dissolved in Fluorinert FC-43 (3M Inc.) of one weight percent (wt%) and spin coated on the carrier substrates in order to form a release layer. This was followed by chemical vapor deposition (CVD) of a 1 μm thick parylene layer (dix-SR, KISCO Ltd.) with a parylene coater (PDS 2010, Specialty Coating Systems). The first metallization layer conductors, the capacitor bottom electrode, and the transistor gate electrodes were inkjet printed with a Dimatix Material Printer (DMP-2831, Fujifilm Dimatix Inc.) using Ag-nanoparticle ink (NPS-JL, Harima Chemicals) with a 10 pl cartridge, 60 μm drop spacing, and a 50 °C stage temperature. The samples were then sintered for one hour at 130 °C. This was followed by CVD of an approximately 150 nm thick parylene layer in order to form the gate and capacitor dielectric. The source, drain, and resistor electrodes were inkjet printed with Ag-nanoparticle ink (NPS-JL) and sintered at 130 °C for one hour. In order to control the spreading of the semiconductor/resistor ink, Teflon fluoropolymer (1 wt% AF1600X in FC-43) surface energy patterns were dispensed using dispenser equipment (Image Master 350 PC, Musashi Engineering) with the following process parameters: 4 kPa discharge pressure, 20 mm/s dispensing speed, a 30 °C syringe, and a 60 °C stage temperature. The samples were immersed in a 20 mM solution of isopropanol and pentafluorobenzenethiol (PFBT; TCI Inc.) for 5 minutes at room temperature to form a self-assembled monolayer that reduces the contact resistance between the source/drain and the organic semiconductor [14]. A solution of 0.2 wt% polystyrene (PS) and 1.0 wt% dithieno[2,3-d;2',3'-d']benzo[1,2-b;4,5-b']dithiophene-C6 (DTBDT-C6) in mesitylene was dispensed to form the p-type organic semiconductor channel for the transistor using the following process parameters: 2 kPa discharge pressure, 20 mm/s dispensing speed, a 30 °C syringe, and a 30 °C stage temperature. This was followed by dispensing 0.2 wt% P3HT in chlorobenzene with the following process parameters: 8 kPa discharge pressure, 20 mm/s dispensing speed, a 30 °C syringe, and a 30 °C stage temperature. Prior to dispensing, the P3HT ink was filtered using a 0.45 μm polytetrafluoroethylene (PTFE) filter. The samples were left at room temperature to planarize before annealing the PS:DTBDT-C6 and P3HT at 100 °C for 15 min. A thin Teflon fluoropolymer (1 wt% AF1600X in FC-43) passivation layer was dispensed on the PS:DTBDT-C6 and P3HT with the following dispensing parameters: 8 kPa discharge pressure, 20 mm/s dispensing speed, a 30 °C syringe, and a 30 °C stage temperature.

B. ELECTRICAL CHARACTERIZATION

The capacitance of the printed capacitors was measured using an LCR meter (ZM2376, NF). The resistance of the printed resistors was measured using a semiconductor parameter analyzer (4200A-SCS, Keithley).

A schematic of the measurement setup used for the electrical characterization of the amplifier is shown in Figure 2. For the measurement of the voltage transfer curves and frequency response, a signal generator (33512B, Keysight) was connected to the input of the charge amplifier while monitoring the input and output with an oscilloscope (3000A, Keysight) and providing the supply voltage with a DC power source (E3640A, Agilent). A custom-made buffer amplifier was connected between the amplifier output and oscilloscope input for impedance matching. This unity gain buffer amplifier had an input impedance of 30 GΩ and output impedance

of 560 Ω. The charge amplification of the proposed printed amplifier was measured by modeling a charge source with a voltage source using a 4.7 nF capacitor connected in series with the output. The measurements were performed in a Faraday gage in order to reduce coupling of external electromagnetic interference to the measurement signals.

C. MICROSCOPY

A confocal laser scanning microscope (OLS3000, Olympus) was used for measuring the lengths of the transistor channels and the lengths and widths of the resistors.

D. PULSE-WAVE MEASUREMENT

The arterial pulse-wave signal was recorded from the radial artery at the distal antebrachium of a healthy 39-year-old male volunteer by using a PVDF-TrFE sensor attached to the wristband setup described in [21]. The signal was sampled at 250 Hz with a 16-bit analog-to-digital converter. An 8.2 nF capacitor was connected in parallel with the sensor in order to decrease the high-pass cut-off frequency of the measurement system. The sensor signal recorded in this experiment was fed to the proposed printed amplifier through a capacitor from a signal generator (33512B, Keysight). The radial augmentation index (rAIx) [22] and reflection index (RI) [23] were extracted from the amplified signal and compared with the same features extracted from the input signal of the amplifier. The feature pointsrequired in the pulse-wave analysis—that is, the amplitudes of early systolic wave P_1, late systolic wave P_2, and diastolic wave B (illustrated in Figure 7)—were calculated as presented in [24]. The two compared parameters are defined as rAIx $= P_2/P_1$ and RI $= B/P_1$.

III. RESULTS AND DISCUSSION

A. THE PRINTED RESISTOR AND CAPACITOR

As mentioned in the introduction, the main issue with printed resistors before was the process variations. Therefore, it is important to understand the different error sources when designing a printed resistor. The resistance of a resistor depends on the resistivity of the material (ρ), together with the resistor's length (L) and cross-sectional area (A), according to the well-known formula:

$$R = \frac{\rho L}{A} = \frac{\rho L}{Wt}, \tag{1}$$

where W is the width and t is the thickness of the resistor. Assuming a uniform annealing process for the resistor material, the variation in resistivity should be minimal and the remaining uncertainty in resistance value should be related to the dimensions of the resistor.

It has previously been shown that the width and length (W/L) of a printed transistor can be controlled with high accuracy by using inkjet-printed parallel source/drain electrodes and a dispensed fluoropolymer bank to control the spreading of the dispensed organic semiconductor ink (a standard deviation of 8 μm and 1 μm was achieved for W and L respectively in [13]). Thus, the same process was adopted for the printed resistor: inkjet-printed parallel Ag electrodes and a dispensed fluoropolymer bank to control the spreading of the dispensed high-resistivity P3HT ink (compare Figure 1's parts (a) and (b)).

TABLE 1. The effect of different error sources on a 1100 micrometer wide and 10 micrometer long P3HT resistor dispensed with 8 kPa pressure.

PARAMETER	ST. DEV.	MEAN	COEFFICIENT OF VARIATION
Length (L)	1 μm	10 μm	10.0%
Width (W)	8 μm	1100 μm	0.7%
Sheet resistance ($R_\square$)	8.21 GΩ/□	57.84 GΩ/□	14.2%
Accumulative			9.1%

In this case, the remaining uncertainty is related to the dispensing process variation. This uncertainty was estimated by dispensing 0.2 wt% P3HT in chlorobenzene on Ag electrodes with ∼1100 μm wide fluoropolymer banks with varying pressures of 6, 8, and 10 kPa (see Figure 3). In order to isolate the effect of dispensing process variation, the measured resistance values were normalized using the width and length of the resistor according to

$$R_\square = \frac{RW}{L}, \tag{2}$$

where $R_\square$ is the sheet resistance, R the measured resistance, W the width of the fluoropolymer bank, and L is the length of the resistor (i.e., the distance between the Ag electrodes). Based on the histogram of sheet resistance values shown in Figure 3, decreasing the dispensing pressure from 10 to 6 kPa increased the sheet resistance from 43.06GΩ/□ to 67.98 GΩ/□. The coefficients of variation for 6, 8, and 10 kPa dispensing pressures are 14.9%, 14.2%, and 16.6% respectively.

Table 1 shows the accumulative effect of different error sources on a printed resistor of 1100 μm width and 10 μm length, and a 8 kPa dispensing pressure, resulting in the designed mean resistance of $R_\mu = 526.1$ MΩ. Since the error sources are independent (L depends on the inkjet printing process, W on the fluoropolymer dispensing process, and t on the P3HT dispensing process), the errors accumulate in quadrature [25] according to:

$$\Delta R = \sqrt{\left(\Delta R_\square \frac{\partial R}{\partial R_\square}\right)^2 + \left(\Delta W \frac{\partial R}{\partial \mathrm{W}}\right)^2 + \left(\Delta L \frac{\partial R}{\partial L}\right)^2}, \tag{3}$$

where Δ denotes the measured standard deviation. The most straightforward way to reduce the accumulative error is to increase the length of the resistor. However, for a given resistance value, doubling the length leads to doubling the width, which may lead to problems if the available circuit area is limited.

The fabrication process for the printed parallel plate capacitors (see Figure 1c) was also adapted from the printed

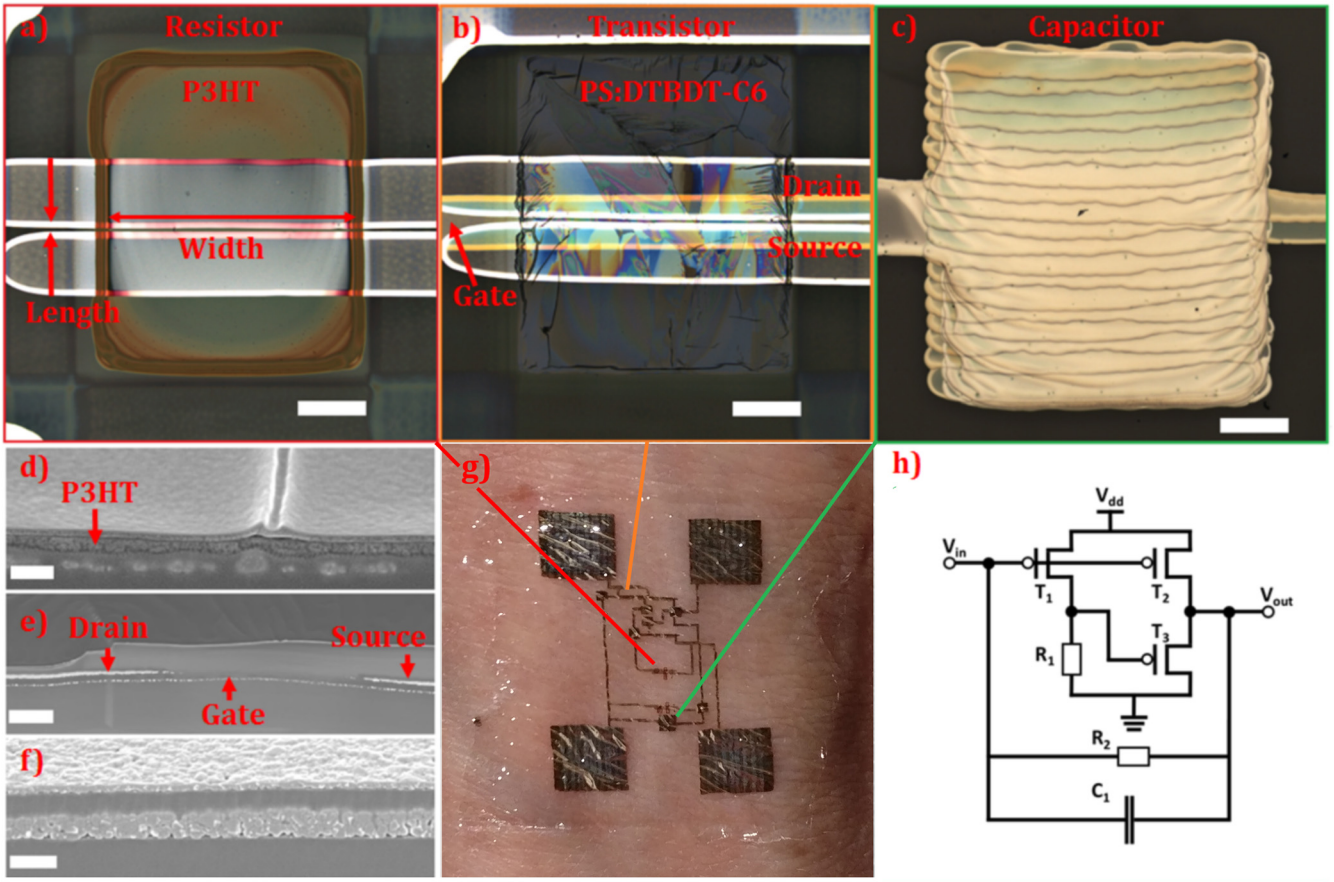

FIGURE 1. Microscope images of the resistor (a), transistor (b), capacitor (c). Cross-section SEM images of the resistor (d), transistor (e) and capacitor (f). An overall image of the charge amplifier attached to the skin at the wrist (g) and charge amplifier circuit (h). The scale bars are 200 μm in (a), (b), and (c); 200 nm in (d); 2 μm in (e); and 400 nm in (f).

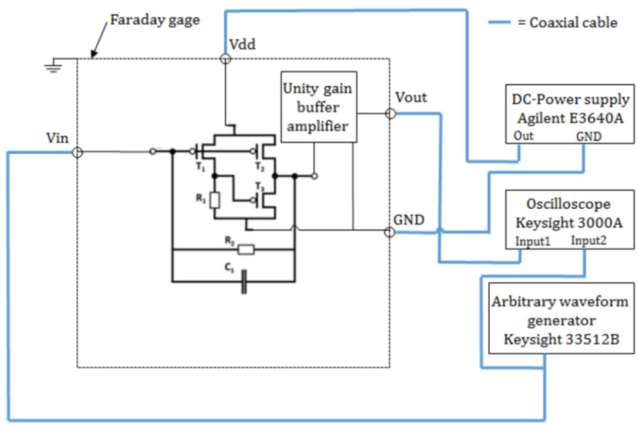

FIGURE 2. The measurement setup used for the electrical characterization of the amplifier.

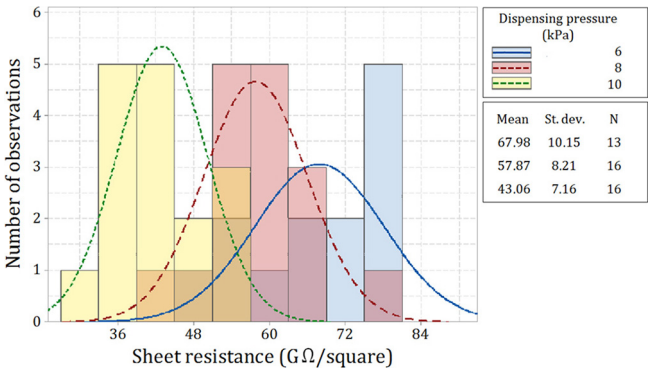

FIGURE 3. The dependence of the resistor sheet resistance on dispensing pressure.

transistor [13] where parylene was used as the gate dielectric. The capacitance of a parallel plate capacitor depends on the permittivity of material ($k\varepsilon_0$), the overlapping area of the electrodes (A), and thickness of the dielectric (d):

$$C = \frac{k\varepsilon_0 A}{\mathrm{d}}. \tag{4}$$

Assuming constant material parameters, the main sources of variation are related to the dimensions of the capacitor. Figure 4 shows the variation in capacitance for two sample sets taken from different process runs; the coefficient of variation is 2.8%. This demonstrates that the thickness of parylene and the overlapping area of the electrodes can be controlled with high accuracy.

The transistor fabrication process was adapted from previous studies [13], [14], [15]. For example, in

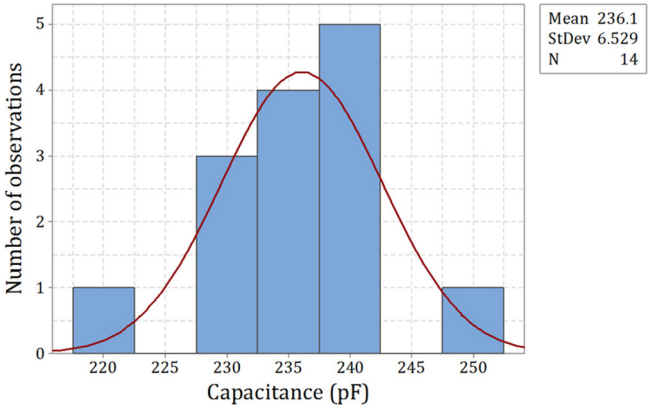

FIGURE 4. A histogram of capacitance values of individual capacitors manufactured in two process runs. Capacitance was measured at 1 kHz.

reference [15] transistors with similar parylene gate dielectric thickness (∼150 nm) and channel length (∼10 μm) were fabricated and characterized. The results showed that the dielectric capacitance per unit area was 24.3 nF/cm^2 at 100 Hz while the mobility was 1.1 cm^2/Vs, threshold voltage −0.26 V, and subthreshold slope 100 mV/dec at 2 V supply voltage. Despite the 150 nm parylene gate dielectric thickness, the gate-source leakage current was less than 10 pA.

B. THE DESIGN OF THE CHARGE AMPLIFIER WITH INTEGRATED RESISTORS AND CAPACITOR

We designed a charge amplifier that was composed of an organic pseudo-CMOS inverter, including a bias resistor (R_1), a feedback resistor (R_2), and a feedback capacitor (C_1). Pseudo-CMOS inverters have the advantages of a higher gain and a wider output voltage range than PMOS inverters and require fewer process steps than CMOS inverters. A small-signal model gives the relationship between input voltage and output voltage as $(V_{out} - V_{offset}) = -A_{open}(V_{in} - V_{offset})$. Considering that the current at the input terminal is equal to the sum of the current through R_2 and C_1:

$$-\frac{dQ}{dt} = \frac{1}{R_2}(V_{in} - V_{out}) - C_1\frac{d}{dt}(V_{in} - V_{out}), \quad (5)$$

we obtain the output voltage:

$$V_{out} = \frac{2\pi ifR_2Q}{(1 - 2\pi ifR_2C_1)\left(1 + A_{open}^{-1}\right)} + V_{offset} \quad (6)$$

as a function of charge Q at the PVDF-TrFE pressure sensor. This formula shows that this charge amplifier has high-pass characteristics with a lower cutoff frequency of

$$f_{LC} = 1/(2\pi R_2C_1) \quad (7)$$

and that the charge-voltage gain A_{charge} above f_{LC} is given by

$$A_{charge} \approx -\frac{A_{open}}{C_1(A_{open} + 1)} \approx -\frac{1}{C_1} \quad (8)$$

if the open-loop gain A_{open} is much higher than unity.

TABLE 2. A comparison between this work and other printed amplifiers.

REFERENCE	YEAR	GAIN	OPERATING VOLTAGE (V)	INTEGRATED BIAS RESISTOR
This work	2019	14	5	Yes
Shiwaku et al. [13]	2017	>10	0.3	No
Ramon et al. [27]	2016	2.3	30	No
Fukuda et al. [28]	2014	1.6	10	No
Kang et al. [29]	2014	9	15	No
Feng et al. [30]	2014	67.3	3	No

C. THE ELECTRICAL CHARACTERIZATION OF THE CHARGE AMPLIFIER

The voltage transfer characteristics (VTCs) of eight fully printed pseudo-CMOS charge amplifiers were measured at 2 V, 3 V, 4 V, and 5 V supply voltage (V_{dd}) levels by sweeping the input voltage (V_{in}) from 0 to $V_{dd} + 0.5$ V while measuring the output voltage (V_{out}). The data was smoothed using a Savitzky-Golay filter with a third-order polynomial in order to reduce the effect of the measurement noise in the clarity of the VTC graphs. The resulting graphs are plotted in Figure 5. The measured range of the transition voltage (V_{trip}) is ∼0.42 V for all V_{dd}, showing uniform behavior of the organic circuits (similar results were previously obtained in [14]). The small-signal gain (dV_{out}/dV_{in}) was then calculated based on the VTC curves. For $V_{dd} = 5$ V, the average small-signal gain was 11.3 with a standard deviation of 2.2 so that the coefficient of variation is ∼20%. A large variation in the small-signal gain is expected because the gain in the first stage of the pseudo-CMOS inverter is proportional to the value of the printed feedback resistor (a 9.1% coefficient of variation; see Table 1).

Based on Table 2, it is apparent that the amplifiers fabricated here compare favorably to other printed amplifiers. The operating voltage can be set between 2 V and 5 V, but reducing it will come at the expense of the gain (as is apparent from Figure 5). Also, it is important to note that the amplifiers presented in this contribution are the only ones in Table 2 that use printed passive components.

The effect of feedback resistance was estimated by printing two amplifiers with different feedback resistances. The frequency responses of these amplifiers are shown in Figure 6. In order to simulate a signal measured with a piezoelectric sensor, a 4.7 nF capacitor was connected in series between the input of the amplifier and the signal generator, as explained in Section II-B.

As can be seen from the amplitude response graph, this transforms the amplifier from a low-pass filter to a band-pass filter where the upper cutoff frequency is governed by the performance of the organic semiconductor (in terms of mobility, contact resistance, etc.) and the lower cut-off frequency by the value of feedback resistor (R_2) and capacitor (C_1), according to Equation (7).

It was possible to adjust the f_{LC} from 320 mHz to 60 mHz by increasing the value of the feedback resistor four fold

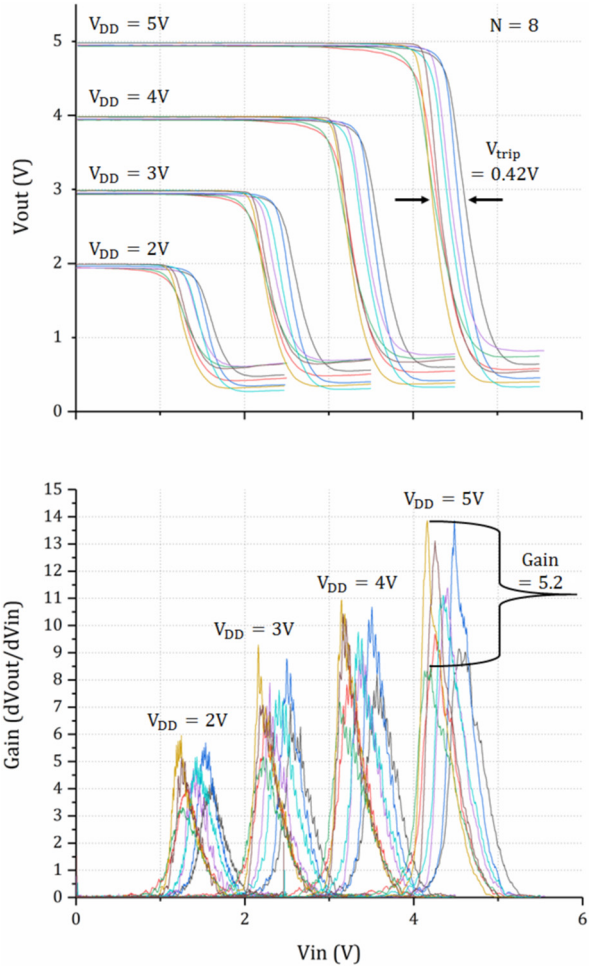

FIGURE 5. The voltage transfer characteristic (VTC) curves of eight fully printed transimpedance amplifiers with different supply voltages and the respective small-signal gains calculated from the VTC curves (Gain = dV_{out}/dV_{in}).

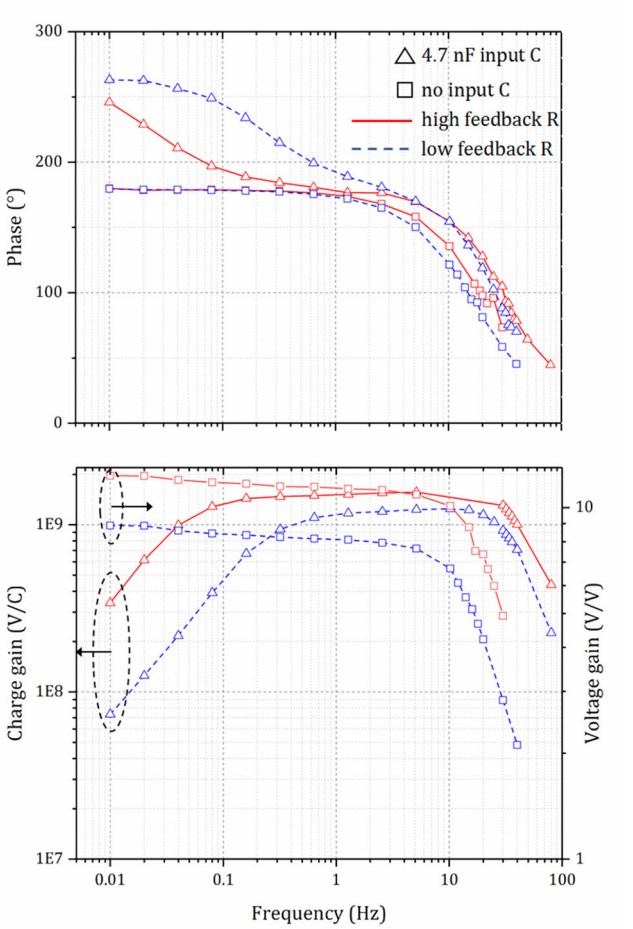

FIGURE 6. The phase and amplitude response of two inverters/charge amplifiers with low- and high-feedback resistances, as well as the response with and without input capacitance.

(i.e., by increasing the distance between the silver electrodes). The upper cutoff frequencies were approximately 36 Hz and 32 Hz for low and high f_{LC} amplifiers respectively. The ability to adjust the f_{LC} is important in many emerging applications of piezoelectric sensors. For example, in the case of arterial pulse-wave measurements, an f_{LC} of ~50 mHz is required to acquire all the important signal features needed for reliable diagnosis [21]. However, higher f_{LC} (lower feedback resistance) reduces the Johnson-Nyquist noise of the feedback resistor so it is important to optimize the f_{LC}. In addition to frequency response measurements, the integrity of the amplifier output signal was verified by comparing it to a fitted sinusoidal function; the coefficient of variation for the residual was approximately 0.8%, proving that the output signal is not distorted.

For amplification of the signal from a piezoelectric sensor, a more useful figure of merit is the charge amplification, which can be calculated as

$$A_{Charge} = \frac{V_{out}}{Q} = \frac{V_{out}}{CV}, \tag{9}$$

where Q is the input charge, $C$is the input capacitor used in the measurement, and V is the amplitude of the input voltage. Charge amplification at the pass band was 1.596V/nC and 1.255V/nC for low- and high-f_{LC} samples respectively. Considering a typical value for PVDF-TrFE d_{33} of −26 pC/N [26], these amplifiers would produce 41 mV/N and 33 mV/N signals.

D. BIOSIGNAL AMPLIFICATION

Lastly, the arterial pulse wave was recorded from the radial artery of the right arm at the distal antebrachium using a PVDF-TrFE sensor attached to a wristband setup that was described in a previous study [21]. The voltage signal generated by the sensor was then fed from the signal generator, through a 9.4 nF capacitor to the f_{LC} = 60mHz transimpedance amplifier.

Figure 7 presents the results of the pulse-wave measurement. Figure 7a shows the inverted input of the amplifier and Figure 7, parts b and c, shows the amplifier output with and without digital low-pass filtering (a cut-off frequency of 10 Hz with a 10th order Butterworth-type filter implemented as forward–backward filtering). In Figure 7c, the

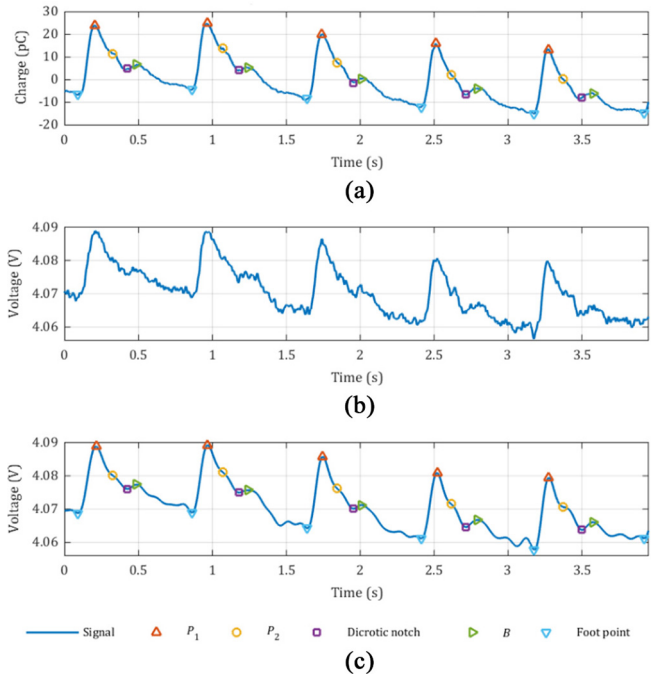

FIGURE 7. An arterial (radial artery) pulse-wave signal recorded using a PVDF-TrFE sensor. The signal is inverted to make comparison easier. The figure shows the input of the amplifier (a), the output of the amplifier (b), and the low-pass–filtered output of the amplifier (c).

TABLE 3. A comparison of the values of the reflection index (RI) and radial augmentation index (rAIx) from the sensor signal and amplifier output.

PARAMETER ($N = 25$)	AVERAGE	ST. DEV
RI, SENSOR	0.388	0.031
RI, OUTPUT	0.404	0.044
RAIX, SENSOR	0.615	0.045
RAIX, OUTPUT	0.626	0.057

feature points of early systolic wave P_1, late systolic wave P_2, the dicrotic notch, and diastolic wave B are also shown. A comparison of the values calculated for rAIx and RI from the sensor signal (Figure 7a) and low-pass–filtered amplifier output (Figure 7c) is presented in Table 3 for a time series based on 25 consecutive pulse waves. Even though the amplifier increases the amount of high-frequency noise in the signal (Figure 7b), this does not significantly distort the actual pulse waveform and the calculated pulse-wave parameters when only the frequency band relevant for pulse-waveform analysis is considered, as demonstrated in Figure 7 and Table 3. The differences between the parameter values extracted from input and output signals are not greater than the natural beat-to-beat variation caused by changing physiological factors.

IV. CONCLUSION

A fully printed ultra-thin charge amplifier with integrated feedback / bias resistors and a feedback capacitor working at a 2 to 5 V operating voltage was demonstrated. The reproducibility of the amplifiers was acceptable, with small transition voltage variation (∼0.42 V) and relatively small signal-gain variation (standard deviation: 2.2). It was shown that the lower cut-off frequency can be controlled by varying the value of the feedback resistor. In addition, an arterial pulse-wave signal measured with a piezoelectric pressure sensor was amplified using the fully printed charge amplifier, and it was shown that the amplified signal contains all the important pulse wave components required for the calculation of clinically relevant indices.

ACKNOWLEDGMENT

The authors thank the Tosoh Corporation for providing the semiconductor material DTBDT-C6.

REFERENCES

[1] G. Yang *et al.*, "Non-invasive flexible and stretchable wearable sensors with nano-based enhancement for chronic disease care," *IEEE Rev. Biomed. Eng.*, vol. 12, pp. 1–34, 2018. doi: 10.1109/RBME.2018.2887301.
[2] S. M. Lee *et al.*, "Self-adhesive epidermal carbon nanotube electronics for tether-free long-term continuous recording of biosignals," *Sci. Rep.*, vol. 4, p. 6074, Aug. 2014.
[3] D.-H. Kim *et al.*, "Epidermal electronics," *Science*, vol. 333, no. 6044, pp. 838–843, Aug. 2011.
[4] J. J. S. Norton *et al.*, "Soft, curved electrode systems capable of integration on the auricle as a persistent brain–computer interface," in *Proc. Nat. Acad. Sci. USA*, vol. 112, no. 13, pp. 3920–3925, Feb. 2015.
[5] S. K. Ameri *et al.*, "Imperceptible electrooculography graphene sensor system for human–robot interface," *npj 2D Mater. Appl.*, vol. 2, p. 19, Jul. 2018.
[6] T. Vuorinen, M.-M. Laurila, R. Mangayil, M. Karp, and M. Mäntysalo, "High resolution E-jet printed temperature sensor on artificial skin," in *Proc. IFMBE EMBEC NBC*, vol. 64, Jun. 2017, pp. 839–842.
[7] T. Mano *et al.*, "Printed organic transistor-based enzyme sensor for continuous glucose monitoring in wearable healthcare application," *ChemElectroChem*, vol. 5, no. 24, pp. 3881–3886, Oct. 2018.
[8] D. Y. Park *et al.*, "Self-powered real-time arterial pulse monitoring using ultrathin epidermal piezoelectric sensors," *Adv. Mater.*, vol. 29, no. 37, Jul. 2017, Art. no. 1702308.
[9] T. Sekine *et al.*, "Fully printed wearable vital sensor for human pulse rate monitoring using ferroelectric polymer," *Sci. Rep.*, vol. 8, p. 4442, Mar. 2018.
[10] Y. Liu, M. Pharr, and G. A. Salvatore, "Lab-on-Skin: A review of flexible and stretchable electronics for wearable health monitoring," *ACS Nano*, vol. 11, no. 10, pp. 9614–9635, Sep. 2017.
[11] M. C. Caccami, M. P. Hogan, M. Alfredsson, G. Marrocco, and J. C. Batchelor, "A tightly integrated multilayer battery antenna for RFID epidermal applications," *IEEE Trans. Antennas Propag.*, vol. 66, no. 2, pp. 609–617, Feb. 2018.
[12] X. Huang *et al.*, "Epidermal radio frequency electronics for wireless power transfer," *Microsyst. Nanoeng.*, vol. 2, Oct. 2016, Art. no. 16052.
[13] R. Shiwaku *et al.*, "Printed organic inverter circuits with ultralow operating voltages," *Adv. Elect. Mater.*, vol. 3, no. 5, Mar. 2017, Art. no. 1600557.
[14] R. Shiwaku *et al.*, "Printed 2 V-operating organic inverter arrays employing a small-molecule/polymer blend," *Sci. Rep.*, vol. 6, Oct. 2016, Art. no. 34726.
[15] R. Shiwaku *et al.*, "A printed organic amplification system for wearable potentiometric electrochemical sensors," *Sci. Rep.*, vol. 8, p. 3922, Mar. 2018.
[16] S. Jung, A. Sou, E. Gili, and H. Sirringhaus, "Inkjet-printed resistors with a wide resistance range for printed read-only memory applications," *Org. Electron.*, vol. 14, pp. 699–702, Jan. 2013.
[17] S. Ali, J. Bae, and C. H. Lee, "Design of versatile printed organic resistor based on resistivity (ρ) control," *Appl. Phys. A, Solids Surf.*, vol. 119, no. 4, pp. 1499–1506, Jun. 2015.
[18] H. Sirringhaus *et al.*, "High-resolution inkjet printing of all-polymer transistor circuits," *Science*, vol. 290, no. 5499, pp. 2123–2126, Dec. 2000.

[19] T. Kawase, T. Shimoda, C. Newsome, H. Sirringhaus, and R. H. Friend, "Inkjet printing of polymer thin film transistors," *Thin Solid Films*, vols. 438–439, pp. 279–287, Aug. 2003.
[20] K.-H. Yin *et al.*, "Controlling electrical properties of conjugated polymers via a solution-based p-type doping," *Adv. Mater.*, vol. 20, no. 17, pp. 3319–3324, Sep. 2008.
[21] M. Peltokangas *et al.*, "Monitoring arterial pulse waves with synchronous body sensor network," *IEEE J. Biomed. Health Inf.*, vol. 18, no. 6, pp. 1781–1787, Nov. 2014.
[22] W. W. Nichols, "Clinical measurement of arterial stiffness obtained from noninvasive pressure waveforms," *Amer. J. Hypertension*, vol. 18, pp. 2–10, Oct. 2004.
[23] S. C. Millasseau, J. M. Ritter, K. Takazawa, and P. J. Chowienczyk, "Contour analysis of the photoplethysmographic pulse measured at the finger," *J. Hypertension*, vol. 24, no. 8, pp. 1449–1456, Feb. 2006.
[24] M. Peltokangas *et al.*, "The effect of percutaneous transluminal angioplasty of superficial femoral artery on pulse wave features," *Comput. Biol. Med.*, vol. 96, pp. 274–282, Apr. 2018.
[25] H. Castrup, "Estimating and combining uncertainties," in *Proc. 8th Annu. ITEA Instrum. Workshop*, May 2004, pp. 1–7.
[26] Piezotech Arkema Group. *TDS Piezotech FC Ink P Datasheet*. Accessed: Jan. 4, 2019. [Online]. Available: https://www.piezotech.eu/en/ Technical-center/Documentation/df
[27] E. Ramon, C. Martínez-Domingo, A. Alcalde-Aragonés, and J. Carrabina, "Development of a simple manufacturing process for all-inkjet printed organic thin film transistors and circuits," *IEEE Trans. Emerg. Sel. Topics Circuits Syst.*, vol. 7, no. 1, pp. 161–170, Mar. 2017.
[28] K. Fukuda *et al.*, "Fully-printed high-performance organic thin-film transistors and circuitry on one-micron-thick polymer films," *Nat. Commun.*, vol. 5, p. 4147, Jun. 2014.
[29] H. Kang *et al.*, "Megahertz-class printed high mobility organic thin-film transistors and inverters on plastic using attoliter-scale high-speed gravure-printed sub-μ gate electrodes," *Org. Electron.*, vol. 15, no. 12, pp. 3639–3647, Dec. 2014.
[30] L. Feng *et al.*, "All-solution-processed low-voltage organic thin-film transistor inverter on plastic substrate," *IEEE Trans. Electron Devices*, vol. 61, no. 4, pp. 1175–1180, Apr. 2014.

MIKA-MATTI LAURILA received the M.Sc. degree in electrical engineering from the Tampere University of Technology, Finland, in 2015. He is currently pursuing the Ph.D. degree with the Printable Electronics Research Group, Tampere University. His research interests are related to the applications of inkjet technology in electronics packaging.

HIROYUKI MATSUI received the M.Sc. degree in applied physics and the D.Sc. degree in advanced materials science from the University of Tokyo, Japan, in 2008 and 2011, respectively. From 2011 to 2013, he was a Project Researcher with the National Institute of Advanced Industrial Science and Technology. From 2013 to 2016, he was an Assistant Professor with the Department of Advanced Materials Science, University of Tokyo. Since 2016, he has been an Associate Professor with the Department of Organic Materials Science, Yamagata University. He has authored over 60 international journal and conference articles. His current research interests include organic electronics, especially organic transistors, solid-state physics, and materials informatics.

REI SHIWAKU received the M.Sc. degree in electrical engineering from Yamagata University, Japan, in 2016, where he is currently pursuing the Ph.D. degree with the Research Center for Organic Electronics. His research interests include organic electronics and printed electronics.

MIKKO PELTOKANGAS received the M.Sc. degree in biomedical engineering from the Tampere University of Technology, Finland, in 2013. He is currently pursuing the Ph.D. degree with the Sensor Technology and Biomeasurements Group, Faculty of Medicine and Health Technology, Tampere University. His research interests are related to noninvasive physiological measurements and the analysis of physiological signals.

JARMO VERHO received the B.Sc. degree in automation from the Tampere University of Technology, Finland, in 2016. He is currently pursuing the M.Sc. degree with the Sensor Technology and Biomeasurements Group, Faculty of Medicine and Health Technology, Tampere University. His research interests include biosignal measurements, low noise electronics, and short-range inductive and radio links.

KAREM LOZANO MONTERO received the B.Sc. degree in electronic systems engineering from the Polytechnic University of Catalonia, Barcelona, Spain, in 2015. She is currently pursuing the M.Sc. degree in electrical engineering with Tampere University, where she is a Research Assistant with the Printable Electronics Research Group. Her research focuses on printed pressure sensors for electronic skin applications.

TOMOHITO SEKINE received the D.Sc. degree in organic materials science from Yamagata University, Japan, in 2016, where he was a Technical Staff Member from 2010 to 2016. He has authored over 30 international journal and conference articles. His current research interests include flexible electronics, especially sensors, actuators, and related materials science.

ANTTI VEHKAOJA received the D.Sc. (Tech.) degree in automation science and engineering from the Tampere University of Technology, Tampere, Finland, in 2015. He has authored over 70 scientific articles. He is currently an Assistant Professor (tenure track) of sensor technology and biomeasurement with Tampere University. His research interests include the development of embedded measurement technologies for physiological monitoring and related signal processing and data analysis methods with a focus on the assessment of vascular condition.

NIKU OKSALA received the M.D. and Ph.D. degrees in medicine and experimental surgery from the University of Eastern Finland in 2000 and 2003, respectively, and the D.Sc. (Med.) degree in molecular biology from Tampere University in 2009. In 2007, he was a Consultant Vascular Surgeon and Clinical Teacher. In 2014, he was an Associate Professor of surgery, being a Tenured Full Professor in 2018. He is currently a Professor of vascular surgery with Tampere University and the Chief Vascular Surgeon with Tampere University Hospital. He has authored over 150 international journal articles. His current research interests include biomedical sensor technology, clinical research, and the molecular biology of atherosclerosis. He serves as a Board Member of the Finnish Cardiovascular Research Center Tampere and the Instrumentarium Science Foundation.

SHIZUO TOKITO received the Doctorate of Engineering and Master of Engineering degrees from the Graduate School of Engineering and Sciences, Kyushu University, Japan, where he became an Assistant Professor. He was a Post-Doctoral Researcher under Prof. A. J. Heeger, Nobel Prize Laureate in Chemistry, with UC Santa Barbara, USA. After that he joined Toyota Central Research and Development Labs Inc., as a Senior Research Engineer and later he joined the Science Technology Research Laboratories of Japan Broadcasting Corporation (NHK) as a Research Director. He is currently the Director and a Distinguished Research Professor with the Research Center for Organic Electronics, Yamagata University. He maintains a large research group of over 60 people, including visiting researchers from many partner companies in industry.

MATTI MÄNTYSALO (M'09) received the M.Sc. and D.Sc. (Tech.) degrees in electrical engineering from the Tampere University of Technology, Tampere, Finland, in 2004 and 2008, respectively. From 2011 to 2012, he was a Visiting Scientist with the iPack Vinn Excellence Center, School of Information and Communication Technology, KTH Royal Institute of Technology, Stockholm, Sweden. He has authored over 100 international journal and conference articles. He is currently a Professor of electronics materials and manufacturing with Tampere University. His current research interests include printed electronics materials, fabrication processes, stretchable electronics, and especially the integration of printed electronics with silicon-based technology (hybrid systems). He was a recipient of the Academy Research Fellow Grant from the Academy of Finland. He has served as the Spokesperson in the IEEE CMPT, the IEC TC119 Printed Electronics Standardization, and the Organic Electronics Association.